Title: Cross-plane transport in a single-molecule two-dimensional van der Waals heterojunction

Authors: Shiqiang Zhao,[1]* Qingqing Wu,[2]* Jiuchan Pi,[1]* Junyang Liu,[1]* Jueting Zheng,[1] Songjun Hou,[2] Junying Wei,[1] Ruihao Li,[1] Hatef Sadeghi,[2] Yang Yang,[1,3]† Jia Shi,[1] Zhaobin Chen,[1] Zongyuan Xiao,[1,3] Colin Lambert,[2]† Wenjing Hong[1,3]†

Affiliations:

[1]State Key Laboratory of Physical Chemistry of Solid Surfaces, iChEM, College of Chemistry and Chemical Engineering & Pen-Tung Sah Institute of Micro-Nano Science and Technology, Xiamen University, Xiamen 361005, China

[2]Department of Physics, Lancaster University, Lancaster LA1 4YB, United Kingdom

[3]Graphene Industry and Engineering Research Institute, Xiamen University, Xiamen 361005, China

*These authors contributed equally to this work.

†Corresponding author. Email: whong@xmu.edu.cn (W.H.); c.lambert@lancaster.ac.uk (C.L.); yangyang@xmu.edu.cn (Y.Y.).

Abstract: Two-dimensional van der Waals heterostructures (2D-vdWHs) stacked from atomically thick 2D materials are predicted to be a diverse class of electronic materials with unique electronic properties. These properties can be further tuned by sandwiching monolayers of planar organic molecules between 2D materials to form molecular 2D-vdW heterojunctions (M-2D-vdWHs), in which electricity flows in a cross-plane way from one 2D layer to the other via a single molecular layer. Using a newly developed cross-plane break junction (XPBJ) technique, combined with density functional theory calculations, we show that M-2D-vdWHs can be created, and that cross-plane charge transport can be tuned by

incorporating guest molecules. More importantly, the M-2D-vdWHs exhibit distinct cross-plane charge transport signatures, which differ from those of molecules undergoing in-plane charge transport.

One Sentence Summary: The cross-plane charge transport are demonstrated in single-molecule two-dimensional van der Waals heterojunctions.

Formatted: Not Highlight

Main Text:

The wide variety of currently available two-dimensional (2D) materials has enabled the stacking of different atomic layers to yield new electronic materials held together by van der Waals (vdW) forces (*1-5*). Despite their early promise (*6*), the preparation of defect-free 2D-vdWHs remains a challenge. To date, 2D-vdWHs have been fabricated using top-down (exfoliation and restacking) and bottom-up (chemical vapor deposition growth, CVD) approaches *(7, 8)*. However, the mechanical transfer of 2D materials is time-consuming and remains technically challenging, while the CVD growth of one 2D material on another requires sophisticated techniques and strict growth conditions (*9*). Methodologies developed for single-molecule electronics offers a unique opportunity for creating M-2D-vdWHs, in which selected molecules are sandwiched between the two 2D-material layers and stabilized by vdW interactions (*10*). For several years, break junction techniques (*11-14*) have been used to trap single molecules between two gold electrodes with sub-angstrom precision. In previous experiments, the molecule is bonded to the electrodes by terminal anchor groups at two ends of the molecule, and electron transport through the molecular junction with an in-plane way (Fig. 1A). In M-2D-vdWHs developed in this work, electrons can transport through the junction in a cross-plane way, i.e., perpendicular to the planes of the 2D materials based on vdW interaction (*15*) (Fig. 1B). Due to the large molecular library (*16-18*) and the variety of responses of molecules to external stimuli (*19-22*), such a transport mode can open new routes

for the fine tuning of charge transport through M-2D-vdWHs. Nevertheless, to date there are no experimental measurements of the cross-plane charge transport due to the lack of a method for fabricating precise M-2D-vdWHs.

To achieve this goal, we develop a cross-plane break junction (XPBJ) technique to fabricate well-defined M-2D-vdWHs with atomic thickness. The XPBJ method was used to construct a large number of graphene-molecule-graphene 2D-vdWHs (graphene M-2D-vdWHs) by repeatedly opening and closing a graphene electrode pair in solution. During the mechanical manipulation of the graphene electrode pair, the cross-plane current was recorded by a current-voltage (*I*-*V*) converter for further statistical analysis. A family of polycyclic aromatic hydrocarbons (PAHs) was selected as the probe molecules (Fig. 1C). Benefiting from their planar structures and the conjugated component therein, these PAHs can couple with graphene electrode and thus allows the fabrication of M-2D-vdWHs (Fig. 1D). Such PAHs are of general interest in molecular electronics because the molecular orbital energy level of them can be tuned by changing the number of phenyl rings (*23, 24*). This XPBJ technique allows the unambiguous and reproducible characterization of charge transport through the cross-plane interfaces of the graphene M-2D-vdWHs, and demonstrates that cross-plane charge transport through M-2D-vdWHs can be tuned by incorporating diverse molecules.

To investigate charge transport through the M-2D-vdWHs, both the microchip and the operational mechanics of the mechanically controllable break junction (MCBJ) (*25*) were redesigned to realize the XPBJ. Two Cu wires coated with CVD-grown single-layer graphene were bent to be O-ring shape, placed in close proximity (~10 μm separation), and fixed on an elastic substrate to serve as the microchip of the break junction technique. During XPBJ measurement, the two graphene electrodes were immersed in a solution containing the target molecules and

brought into contact with each other by a downward bending of the substrate. The direction of the actuator movement was switched when the measured conductance reached either a high conductance value of $10^{-2.5}$ G_0 (where G_0 is quantum conductance, ~245.4 nS) or a low conductance value of $10^{-7.5}$ G_0 (≈0 nS). The pre-set high value prevents damage of the graphene layer or the formation of a Cu-Cu contact, while the low value prevents the recording of insignificant noise data. Fig. 1E shows the individual conductance traces recorded with this modified MCBJ technique (Fig. S2) using a 100 mV bias voltage in solutions containing the target molecules, and that recorded in the pure solvent. For the pure solvent, the individual conductance traces contain no discernible plateau (Fig. 1E). In contrast, in the presence of PAH molecules, there emerged clear plateaus in the conductance traces in the conductance range between 10^{-3} G_0 (~77.6 nS) and 10^{-6} G_0 (~0.1 nS). To obtain the statistics, more than 1000 conductance traces were collected for pure solvent and each of the PAH molecules. The plateaus contributed to the distinct peaks in their corresponding one-dimensional conductance histograms (Fig. 1, F and G), and the intensified conductance clouds in two-dimensional conductance-distance histograms (Fig. S4), suggesting the formation of single graphene-molecule-graphene junctions (*12*). It is found that PAH 6" provides the highest conductance at $10^{-3.66}$ G_0 (~17.0 nS), which is about ~60 times higher than the lowest conductance from PAH 2 at $10^{-5.46}$ G_0 (~0.3 nS).

To investigate the dependence on the cross-plane area of these molecular junctions, the measured conductances were plotted as a function of the number of benzene rings, as shown in Fig. 1H. In conventional in-plane single-molecule junctions, where the current flows in the plane of the molecular backbone, the conduction decreases when the length of the molecule increases because the molecules act as tunnel barriers (*26, 27*). In contrast, in our experiments the shortest molecule PAH 2 has the lowest conductance (Fig. 1H). This observation shows that the geometries

of the as-fabricated graphene-molecule-graphene junctions are M-2D-vdWHs, where the target molecules lie flat on the surface of the graphene electrode and create a cross-plane conduction path (Fig. 1D, red arrows). With this framework, an increase in conductance with the number of benzene rings is expected (Fig. 1, F and G), because of the corresponding increase in the cross-plane area. Classically, if Ohm's law is applicable, the conductance should scale with the number of benzenes. However, the measured exponential dependence of the conductance on the number of benzene rings for linear PAH molecules is completely non-classical, and significantly, for two PAH molecules with the same number of benzene rings, their conductances are different (Fig. 1H). For instance, the conductance of PAH 4 ($10^{-4.61}$ G_0, ~1.9 nS) is around 50% higher than that of PAH 4' ($10^{-4.82}$ G_0, ~1.2 nS), molecular topological dependent conductance further suggests room-temperature quantum transport.

To determine the microscopic structures of the M-2D-vdWHs, we constructed the two-dimensional conductance-distance histogram for the graphene M-2D-vdWHs with PAHs, and then statistically analyzed their single-molecule conductance features (*28*). Fig. 2A gives the 2D-histogram for the graphene M-2D-vdWHs with PAH 3, while Fig. 2B shows the displacement distributions for six typical graphene M-2D-vdWHs. The measurement results for the pure solvent and all the other PAHs are given in Figs. S5 and S7. In comparison with the control experiment of pure solvent, it was inferred that the peak at about 0.27 nm arises from the direct tunneling between the two graphene electrodes (*29*), and the latter one is attributed to the graphene M-2D-vdWHs with PAH 3. As PAH 3 can be viewed as a graphene nanoribbon, the thickness of PAH 3 is approximately the same as the single-layer graphene sheet (~ 1.0 nm) (*30*), which agrees well with the probable plateau length measured in our experiment. The most probable plateau lengths for the PAH molecules lie in 0.87~1.08 nm (Fig. 2B and Fig. S6, A-C). These values are considerably

smaller than the molecular lengths of the PAH molecules, and comparable with the spacing between two graphene layers incorporated with PAH molecules (Fig. S6 and Table S2). This observation verified the cross-plane model of charge transport in the graphene M-2D-vdWHs (Fig. 1B). Moreover, we performed the single-molecule conductance measurement with different concentrations. As shown in Fig. S8, the formation probability of M-2D-vdWHs is dependent on the concentration, while the measured conductance value is independent of the concentration, which shows that the conductance characterization comes from single probe molecule.

To further understand the microscopic configurations of the as-fabricated junctions, Raman spectroscopy (*31*) was employed to investigate the molecule assembled on graphene electrodes. For each of the other spectra acquired in the presence of the target molecules, there is a significant peak at 1529 cm^{-1} (Fig. 2C). Neither the graphene nor the target molecule alone exhibits this peak (Fig. S9). Thus, this signal is attributed to the adsorption of target molecules on the graphene surface. A previous report demonstrated that this signal is also an indicator of single-layer graphene because this signal is absent in the Raman spectra in the case of aromatic molecules absorbed on graphite or multilayer graphene (*32*). The ratio of the intensities of the G and 2D peaks as a function of the number of benzene rings was plotted in Fig. 2D. This ratio is determined by the electron concentration of graphene after doping and therefore shows the level of doping (*33*), thus the decreasing curve indicates that the degree of charge transport between each target molecule and the graphene electrode increases as the number of benzene rings increases (Fig. 2D), which agrees well with the path analysis of the graphene M-2D-vdWHs depicted in Fig. 1H. To assess whether the graphene layer is able to retain itself during the XPBJ experiments, we had characterized the graphene electrodes before and after XPBJ experiments (Fig. S9). It is found that in the two Raman spectra the 2D peaks are quite sharp and there is no discernible difference

between them (see Table S3 for further information), which indicates that there is a high-quality graphene layer on the copper wires, all through the XPBJ operation (*34*).

To elucidate the nonlinear conductances increase of graphene M-2D-vdWHs with the number of benzene rings, we calculated their cross-plane conductances using a combination of the ab initio density function theory package SIESTA (*35*) and the quantum transport code Gollum (*36*). Fig. 3A shows the model of cross-plane graphene M-2D-vdWHs used in the calculations. Each sheet extends to +/- infinity in the z-direction, and the structure is regarded as a four-probe device, in which the cross-plane current injected from lead 1 is collected by leads 3 and 4. To avoid edge effects, the graphene sheets are assigned periodic boundary conditions in the x-direction. The PAHs lie between the two graphene sheets with a separation varying from 3.3 to 3.5 Å depending on the AA, AB or intermediate nature of the stacking between the sandwiched molecule and the graphene sheets (Figs. S10 and S11). We calculated the binding energy E_{b} for these stacking configurations using a basis set superposition error (BSSE) correction (*37, 38*), where $E_{\mathrm{b}} = \mathrm{E[AB]} - \mathrm{E[Ab]} - \mathrm{E[aB]}$, and found that AB stacking is the most favorable configuration (see Fig. S12 for further details). The distance between the adsorbed molecule and graphene and the magnitude of binding energy are in qualitative agreement with the literature values (*39*).

After extracting the resulting mean-field Hamiltonian and overlap matrices, we computed the electrical properties of the devices using the quantum transport code Gollum (*36*) (more details can be seen in Methods). Fig. 3B shows the calculated average conductances of linear PAHs stemming from the electron transport from lead 1 to leads 3 and 4 as a function of the Fermi energy E_{F}. More details and conductances of other PAHs are presented in Figs. S12 and S13. The conductances are weighted by Boltzmann factors based on binding energies of AA, AB stacking and one intermediate stacking configuration (see Figs. S10, S11 and Section 7 in Supplementary

Materials). In agreement with our experimental values, the conductances for linear PAHs (PAH 2, PAH 3, PAH 4, and PAH 5) increase approximately exponentially with the number of benzene rings over a wide range of Fermi energies E_F near the DFT-predicted Fermi energy E_F^{DFT} of a pristine graphene sheet. Although the precise value of E_F depends on the doping of the graphene in contact with the Cu wires, qualitative agreement with the experimental result was obtained even at the ideal DFT-predicted value. The agreement between the calculated (light blue dots) and the measured (brown dots) conductance values show clear evidence that cross-plane transport is quantum mechanical in nature and takes place via phase-coherent tunneling. Furthermore, we find that different shapes of the same area lead to different conductances (Fig. 3C). These findings are in contrast with a classical picture of cross-plane transport, where the conductance is expected to increase in proportion to the area, or equivalently the number of benzene rings. More importantly, the geometries of M-2D-vdWHs are entirely different from junctions fabricated with conventional metallic electrodes. In the case of PAHs, it was recently observed that the molecular junctions adopt “sandwich compound” compact geometries when using either Ag or Pt electrodes (*24*). However, although the sandwiched molecules there are also flat, the PAHs in these devices bind to the metallic electrodes with a covalent bond and exhibit conventional in-plane transport. It is also reported that the conductance decreases from naphthalene to anthracene with thiophenyl anchor in traditional MCBJ that involved with Au electrodes (*40*). Similar results are reproduced in our in-pane calculations shown by the magenta dots in Fig. 3C (see Fig. S14 for details). In contrast, in the M-2D-vdWHs studied here, the PAHs couple electronically to the graphene electrodes via π-π stacking interactions and electricity flows via cross-plane transport, in which all the components of the sandwiched molecules are active, i.e., all the benzene rings are directly coupled to the graphene electrodes.

To conclude, for the first time, we report the fabrication of single two-dimensional van der Waals heterojunctions with atomic thickness using a newly developed cross-plane break junction technique. Thousands of graphene M-2D-vdWHs were repeatedly fabricated, allowing the measurement of cross-plane charge transport through van der Waals heterojunction with 2D materials for the first time. By employing a family of PAHs as model molecules, we found that their cross-plane charge transport is distinct from the conventional in-plane charge transport. It is shape ~~dependence~~ dependent and shows a non-classical increase in conductance with the area. Comparison between theory and experiment~~,~~ clearly demonstrat~~inges~~ that room-temperature, cross-plane transport is quantum mechanical ~~and~~, takes place via phase-coherent ~~tunneling~~tunnelling and involves $\pi - \pi$ overlap between the electrodes and all the benzene rings in the molecules. Importantly, this result suggests that in the future, strategies based on tuning the electronic properties of sandwiched molecules can be used to control cross-plane transport. The 2D-vdWHs devices and the versatile fabrication technique developed in this work can be extended to various molecular materials and opens new opportunities for exploiting the chemistry, design, fabrication, and characterization of molecular 2D materials with van der Waals heterostructures.

References and Notes

1. K. S. Novoselov, A. Mishchenko, A. Carvalho, A. H. Castro Neto. 2D materials and van der Waals heterostructures. *Science* **353**, aac9439 (2016).
2. M. EI Abbassi, S. Sangtarash, X. Liu, M. L. Perrin, O. Braun, C. Lambert, H. S. J. van der Zant, S. Yitzchaik, S. Decurtins, S.-X. Liu, H. Sadeghi, M. Calame, Robust graphene-based molecular devices. *Nat. Nanotechnol.* **14**, 957-961 (2019).
3. M. Famili, C. Jia, X. Liu, P. Wang, I. M. Grace, J. Guo, Y. Liu, Z. Feng, Y. Wang, Z. Zhao4 S. Decurtins, R. Haner, Y. Huang, S.-X. Liu, C. J. Lambert, X. Duan, Self-assembled molecular-electronic films controlled by room temperature quantum interference. *Chem* **5**, 474-484 (2019).
4. C. Jia, M. Famili, M. Carlotti, Y. Liu, P. Wang, I. M. Grace, Z. Feng, Y. Wang, Z. Zhao, M. Ding, X. Xu, C. Wang, S.-J. Lee, Y. Huang, R. C. Chiechi, C. J. Lambert, X. Duan, Quantum interference mediated vertical molecular tunneling transistors. *Sci. Adv.* **4**, eaat8237 (2018).
5. H. Wen, W. Li, J. Chen, G. He, L. Li, M. A. Olson, A. C.-H. Sue, J. F. Stoddart, X. Guo, Complex formation dynamics in a single-molecule electronic device. *Sci. Adv.* **2**, e1601113

(2016).
6. F. Withers, O. D. Pozo-Zamudio, A. Mishchenko1, A. P. Rooney, A. Gholinia, K. Watanabe, T. Taniguchi, S. J. Haigh, A. K. Geim, A. I. Tartakovskii, K. S. Novoselov, Light-emitting diodes by band-structure engineering in van der Waals heterostructures. *Nat. Mater.* **14**, 301-306 (2015).
7. X. Li, W. Cai, J. An, S. Kim, J. Nah, D. Yang, R. Piner, A. Velamakanni, I. Jung, E. Tutuc, S. K. Banerjee, L. Colombo, R. S. Ruoff, Large-area synthesis of high-quality and uniform graphene films on copper foils. *Science* **324**, 1312-1314 (2009).
8. L. Yan, Y. B. Zheng, F. Zhao, S. Li, X. Gao, B. Xu, P. S. Weiss, Y. Zhao, Chemistry and physics of a single atomic layer: strategies and challenges for functionalization of graphene and graphene-based materials. *Chem. Soc. Rev.* **41**, 97-114 (2012).
9. M. Xu, T. Liang, M. Shi, H. Chen, Graphene-Like Two-Dimensional Materials. Chen, *Chem. Rev.* **113**, 3766-3798 (2013).
10. E. Lörtscher, Wiring molecules into circuits. *Nat. Nanotechnol.* **8**, 381-384 (2013).
11. M. A. Reed, C. Zhou, C. J. Muller, T. P. Burgin, J. M. Tour, Conductance of a molecular junction. *Science* **278**, 252-254 (1997).
12. B. Xu, N. J. Tao, Measurement of single-molecule resistance by repeated formation of molecular junctions. *Science* **301**, 1221-1223 (2003).
13. G. K. Ramachandran, T. J. Hopson, A. M. Rawlett, L. A. Nagahara, A. Primak, S. M. Lindsay, A bond-fluctuation mechanism for stochastic switching in wired molecules. *Science* **300**, 1413-1416 (2003).
14. L. Rincón-García, C. Evangeli, G. Rubio-Bollinger, N. Agraït, Thermopower measurements in molecular junctions. *Chem. Soc. Rev.* **45**, 4285-4306 (2016).
15. S. Wu, M. T. González, R. Huber, S. Grunder, M. Mayor, C. Schönenberger, M. Calame, Molecular junctions based on aromatic coupling. *Nat. Nanotechnol.* **3**, 569-574 (2008).
16. L. Venkataraman, J. E. Klare, C. Nuckolls, M. S. Hybertsen, M. L. Steigerwald, Dependence of single-molecule junction conductance on molecular conformation. *Nature* **442**, 904 (2006).
17. S. H. Choi, B. Kim, C. D. Frisbie, Electrical resistance of long conjugated molecular wires. *Science* **320**, 1482-1486 (2008).
18. C. Guo, K. Wang, E. Zerah-Harush, J. Hamill, B. Wang, Y. Dubi, B. Xu, Molecular rectifier composed of DNA with high rectification ratio enabled by intercalation. *Nat. Chem.* **8**, 484-490 (2016).
19. H. Song, Y. Kim, Y. H. Jang, H. Jeong, M. A. Reed, T. Lee, Observation of molecular orbital gating. *Nature* **462**, 1039-1043 (2009).
20. A. C. Aragonès, N. L. Haworth, N. Darwish, S. Ciampi, N. J. Bloomfield, G. G. Wallace, I. Diez-Perez, M. L. Coote, Electrostatic catalysis of a Diels-Alder reaction. *Nature* **531**, 88-91 (2016).
21. C. Jia, A. Migliore, N. Xin, S. Huang, J. Wang, Q. Yang, S. Wang, H. Chen, D. Wang, B. Fen, Z. Liu, G. Zhang, D.-H. Qu, H. Tian, M. A. Ratner, H. Q. Xu, A. Nitzan, X. Guo, Covalently bonded single-molecule junctions with stable and reversible photoswitched conductivity. *Science* **352**, 1443-1445 (2016).
22. N. Xin, J. Guan, C. Zhou, X. Chen, C. Gu, Y. Li, M. A. Ratner, A. Nitzan, J. F. Stoddart, X. Guo, Concepts in the design and engineering of single-molecule electronic devices. *Nat. Rev. Phys.* **1**, 211-230 (2019).
23. F. Chen, N. J. Tao, Electron Transport in Single Molecules: From Benzene to Graphene. *Acc. Chem. Res.* **42**, 429-438 (2009).

24. T. Yelin, R. Korytár, N. Sukenik, R. Vardimon, B. Kumar, C. Nuckolls, F. Evers, O. Tal, Conductance saturation in a series of highly transmitting molecular junctions. *Nat. Mater.* **15**, 444-449 (2016).
25. W. Hong, H. Valkenier, G. Mészáros, D. Z. Manrique, A. Mishchenko, A. Putz, P. M. García, C. J. Lambert, J. C. Hummelen, T. Wandlowski, An MCBJ case study: the influence of pi-conjugation on the single-molecule conductance at a solid/liquid interface. *Beilstein J. Nanotechnol.* **2**, 699-713 (2011).
26. B. Kim, S. H. Choi, X. Y. Zhu, C. D. Frisbie, Molecular tunnel junctions based on π-conjugated oligoacene thiols and dithiols between ag, au, and pt contacts: effect of surface linking group and metal work function. *J. Am. Chem. Soc.* **133**, 19864-19877 (2011).
27. H. Rascón-Ramos, J. M. Artés, Y. Li, J. Hihath, Binding configurations and intramolecular strain in single-molecule devices. *Nat. Mater.* **14**, 517–522 (2015).
28. J. Zheng, J. Liu, Y. Zhuo, R. Li, X. Jin, Y. Yang, Z.-B. Chen, J. Shi, Z. Xiao, W. Hong, Z.-Q. Tian, Electrical and SERS detection of disulfide-mediated dimerization in single-molecule benzene-1,4-dithiol junctions. *Chem. Sci.* **9**, 5033-5038 (2018).
29. Z. Tan, D. Zhang, H.-R. Tian, Q. Wu, S. Hou, J. Pi, H. Sadeghi, Z. Tang, Y. Yang, J. Liu, Y.-Z. Tan, Z.-B. Chen, J. Shi, Z.Xiao, C. Lambert, S.-Y. Xie, W. Hong, Atomically defined angstrom-scale all-carbon junctions. *Nat. Commun.* **10**, 1748 (2019).
30. Y. Liu, Y. Huang, X. Duan, Van der Waals integration before and beyond two-dimensional materials. *Nature* **567**, 323-333 (2019).
31. J. F. Li, Y. F. Huang, Y. Ding, Z. L. Yang, S. B. Li, X. S. Zhou, F. R. Fan, W. Zhang, Z. Y. Zhou, D. Y. Wu, B. Ren, Z. L. Wang, Z. Q. Tian, Shell-isolated nanoparticle-enhanced Raman spectroscopy. *Nature* **464**, 392-395 (2010).
32. X. Dong, Y. Shi, Y. Zhao, D. Chen, J. Ye, Y. Yao, F. Gao, Z. Ni, T. Yu, Z. Shen, Y. Huang, P. Chen, L.-J. Li, Symmetry breaking of graphene monolayers by molecular decoration. *Phys. Rev. Lett.* **102**, 135501 (2009).
33. A. Das, B. Pisana, Chakraborty, S. Piscanec, S. K. Saha, U. V. Waghmare, K. S. Novoselov, H. R. Krishnamurthy, A. K. Geim, A. C. Ferrari, A. K. Sood, Monitoring dopants by Raman scattering in an electrochemically top-gated graphene transistor. *Nat. Nanotechnol.* **3**, 210-215 (2008).
34. A. C. Ferrari, J. C. Meyer, V. Scardaci, C. Casiraghi, M. Lazzeri, F. Mauri, S. Piscanec, D. Jiang, K. S. Novoselov, S. Roth, A. K. Geim. Raman spectrum of graphene and graphene layers. *Phys. Rev. Lett.* **97**, 187401 (2006)
35. J. M. Soler *et al.*, *J. Phys. Condens. Matter* **14**, 2745-2779 (2002).
36. J. Ferrer, C. J. Lambert, V. M. García-Suárez, D. Z. Manrique, D. Visontai, L. Oroszlany, R. Rodríguez-Ferradás, I. Grace, S. W. D. Bailey, K. Gillemot, H. Sadeghi, L. A. Algharagholy, GOLLUM: a next-generation simulation tool for electron, thermal and spin transport. *New J. Phys.* **16**, 093029 (2014).
37. Brauer, M. K. Kesharwani, J. M. L. Martin, Some observations on counterpoise corrections for explicitly correlated calculations on noncovalent interactions. *J. Chem. Theory Comput.* **10**, 3791-3799 (2014).
38. K. Wang, A. Vezzoli, I. M. Grace, M. McLaughlin, R. J. Nichols, B. Xu, C. J. Lambert, S. J. Higgins, Charge transfer complexation boosts molecular conductance through Fermi level pinning. *Chem. Sci.* **10**, 2396-2403 (2019).
39. S. D. Chakarova-Käck, E. Schröder, B. I. Lundqvist, D. C. Langreth, Application of van der Waals density functional to an extended system: adsorption of benzene and naphthalene on

graphite. *Phys. Rev. Lett.* **96**, 146107 (2006).
40. V. Kaliginedi, P. Moreno-García, H. Valkenier, W. Hong, V. M. García-Suárez, P. Buiter, J. L. H. Otten, J. C. Hummelen, C. J. Lambert, T. Wandlowski, Correlations between Molecular Structure and Single-Junction Conductance: A Case Study with Oligo(phenylene-ethynylene)-Type Wires. *J. Am. Chem. Soc.* **134**, 5262-5275 (2012).

Acknowledgements This research was supported by the National Key R&D Program of China (2017YFA0204902), National Natural Science Foundation of China (21722305, 21973079, 21673195, 61573295, 21933012, 21703188), Natural Science Foundation of Fujian Province (23186006), China Postdoctoral Science Foundation (2017M622060), for funding work in Xiamen. This work is supported by FET Open project 767187-QuIET, the EU project BAC-TO-FUEL and the UK EPSRC grants EP/N017188/1, EP/M014452/1 in Lancaster. **Author Contributions** W. H., Y.Y., and C. L. designed the experiments and co-supervised the project. W. H., Y.Y., C. L., S. Z., and Q. W. wrote the manuscript with input from all authors. S. Z., J. P., Y.Y., J. L., and J. W carried out the break junction experiments and analysed the data. W. H., J. S., Z. C., and R. L. built the electrical measurement instrument and wrote the software to control the break junction setup. J. Z., S. Z., and Z. X. prepared the graphene microchip and optimised the break junction setup. Q. W., S. H., H. S., C. L., and performed the theoretical modelling. All authors have given approval to the final version of the manuscript; **Author information**: Reprints and permissions information is available at www.science.com/reprints. The authors declare no competing financial interests. Readers are welcome to comment on the online version of the paper; and **Data and materials availability**: The data that support the findings of this study are available from the corresponding author upon reasonable request.

Supplementary Materials

Materials and Methods

Figs. S1-S14

Tables S1-S3

References (*41-42*)

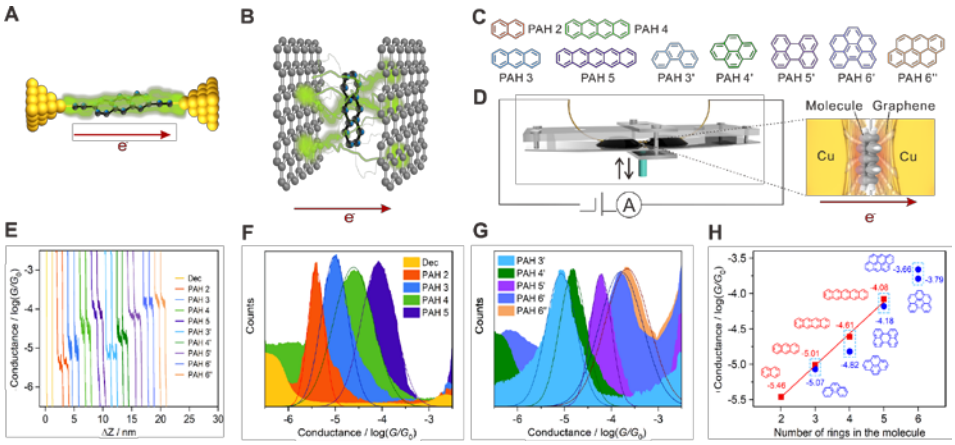

Fig.1. Fabrication and charge transport characterization of graphene M-2D-vdWHs. Illustrations of in-plane (**A**) and cross-plane (**B**) charge transport. Green trajectories are indicative of electron scattering paths. (**C**) Chemical structures of the PAHs that sandwiched between two graphene electrodes. Particularly, naphthalene (PAH 2), anthracene (PAH 3), tetracene (PAH 4) and pentacene (PAH 5) are linear PAHs, while phenanthrene (PAH 3'), pyrene (PAH 4'), perylene (PAH 5'), benzoperylene (PAH 6') and anthanthrene (PAH 6'') are nonlinear PAHs. (**D**) Schematic of the XPBJ technique and the device structure of the studied graphene M-2D-vdWHs. (**E**) Examples of conductance versus displacement traces measured with PAHs and traces measured without the PAHs (yellow, Dec). The traces are shifted horizontally for clarity. One-dimensional conductance histograms generated from ~1000 traces for graphene M-2D-vdWH of the linear PAHs (**F**) and the nonlinear PAHs (**G**). (**H**) The single-molecule conductance of the each graphene M-2D-vdWH, plotted as a function of the number of benzene rings of the sandwiched molecule.

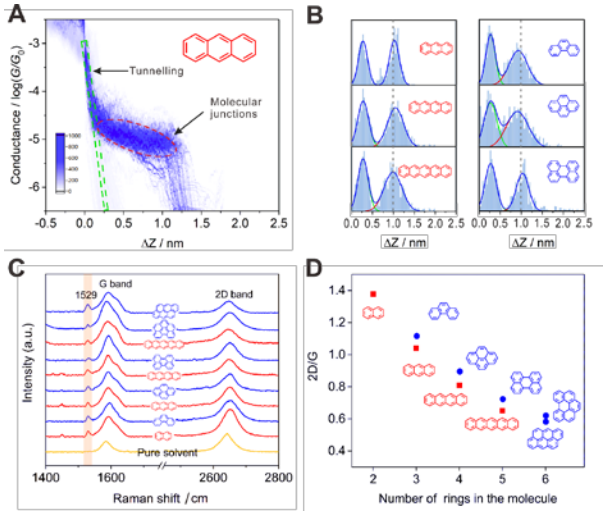

Fig. 2. Displacement and Raman characterization of the graphene M-2D-vdWHs. (**A**) The two-dimensional conductance-distance histogram for the graphene M-2D-vdWHs with PAH 3. The green rectangular dotted frame represents tunneling in decane, and the red elliptical dotted frame represents molecular junctions. (**B**) The relative displacement distributions for the graphene M-2D-vdWHs with PAH 3, PAH 4, PAH 5, PAH 3', PAH 4' and PAH 5'. (**C**) Raman spectrum of the graphene electrode pair that experienced XPBJ operation in the presence of pure solvent (the yellow curve), and the Raman spectra of the graphene M-2D-vdWHs fabricated by the XPBJ method. The sandwiched molecules of the graphene M-2D-vdWHs are PAHs. (**D**) The ratio of the intensities of the G and 2D peaks as a function of the number of benzene rings.

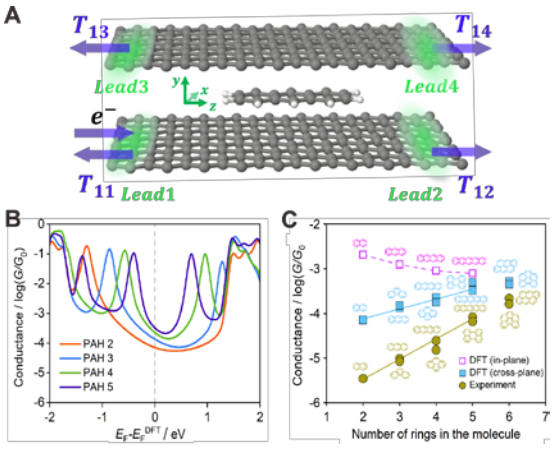

Fig. 3. Theoretical simulations for the charge transport in the graphene M-2D-vdWHs. (**A**) Schematic of the graphene M-2D-vdWHs, where PAH 3 is sandwiched between two graphene sheets, used in the calculations. Electrons are injected from lead 1. T_{11} is the reflection coefficient, while T_{12}, T_{13}, and T_{14} are transmission coefficients into the other three terminals. (**B**) Boltzmann-weighted average conductances collected from the grey curves of Fig. S12 as a function of the Fermi level relative to that predicted by DFT. The Fermi energy is depicted by the grey vertical dashed line which is estimated by DFT. Those average conductances are calculated based on binding energies and derived from transmission functions (obtained from the sum of the transmission coefficients $T_{13}+T_{14}$) by formula 3-8 of Section 7.1 in Supplementary Materials. The results of linear PAHs are displayed for a tidy and clear view while those of all the PAHs are shown in Fig. S12. (**C**) Conductances at Fermi energy from DFT calculations and those from the experiment. The brown dots show the experimental values, while the light blue dots represent the theoretical results for graphene M-2D-vdWHs junctions. The magenta is the conductance of linear PAHs in gold-gold break junctions with in-plane transport (Fig. S14).